AIAA JOURNAL
Vol. 43, No. 7, July 2005

Boundary-Layer Dispersion of Near-Wall Injected Particles of Various Inertias

A. J. Dorgan,* E. Loth,† and T. L. Bocksell‡
University of Illinois at Urbana–Champaign, Urbana, Illinois 61801-2953
and
P. K. Yeung§
Georgia Institutue of Technology, Atlanta, Georgia 30332-0150

A direct numerical simulation approach was employed along with a Lagrangian particle tracking technique to investigate dilute particle motion and dispersion in a horizontal turbulent boundary layer ($Re_\tau = 270$) with no streamwise pressure gradient. Particle inertias based on inner Stokes numbers St^+ (based on friction velocity) ranging from 10^{-2} to 10^2 were investigated. The particles were injected near the wall at a height of four wall units (with elastic wall collision specified at one wall unit), and the terminal velocity was kept small so that particle–eddy interaction would be the primary dispersion. The results showed that particles having $St^+ < 1$ behave approximately as fluid tracers with respect to the large-scale turbulent structures. Particles with a significant inertia effect ($St^+ > 1$) tended to yield increased near-wall concentrations and wall collisions, qualitatively consistent with previous channel flow experiments and simulations, but particle bounce velocities were significantly different due to wall reflections and near-wall injection. Lagrangian statistics of the transverse fluid velocity deviated substantially from the Eulerian statistics due to asymmetric diffusion. In addition, particle relative velocities far exceeded the terminal velocity for moderate and large inertia particles, which was explained by a simple theoretical model.

Nomenclature

C	=	mean Eulerian particle concentration
C_D	=	drag coefficient
d	=	diameter
$\boldsymbol{F}_D$	=	drag force
$\boldsymbol{F}_g$	=	gravitational force
f	=	frequency
g	=	magnitude of gravitational acceleration
k	=	turbulent kinetic energy
L_x, L_y, L_z	=	dimensions of computational domain in Cartesian directions
m	=	mass
Re	=	Reynolds number
St	=	Stokes number
t	=	time
u, v, w	=	streamwise, transverse/vertical, and spanwise velocity components
$V, \boldsymbol{V}$	=	velocity vector, magnitude
x, y, z	=	streamwise, transverse/vertical, and spanwise coordinates
γ	=	drift parameter
δ	=	reference boundary-layer thickness (thickness at injection location)
ε	=	turbulent dissipation per unit mass
ν	=	kinematic viscosity
ρ	=	density
τ	=	timescale
τ_{dom}	=	average time a particle requires to traverse particle tracking domain
τ_{int}	=	total integration time

Subscripts

bounce	=	particle–wall collision
f	=	fluid quantity
p	=	particle quantity
rel	=	particle quantity relative to the fluid
term	=	based on terminal velocity
δ	=	based on outer scales
Λ	=	based on Lagrangian turbulence scales
τ	=	based on wall-shear stress
0	=	injection location
∞	=	freestream

Superscripts

$-$	=	Eulerian-averaged quantity
$'$	=	fluctuation about the Eulerian average
$+$	=	based on inner scales
$*$	=	nondimensional length based on δ

Received 11 March 2004; revision received 28 November 2004; accepted for publication 29 November 2004.

*Research Assistant, Aerospace Engineering Department. Member AIAA.

†Professor, Aerospace Engineering Department, 306 Talbot Laboratory, 104 South Wright Street; e-loth@uiuc.edu. Associate Fellow AIAA.

‡Ph.D. Student, Aerospace Engineering Department; currently Senior Engineer, MS 184-42, Pratt and Whitney, 400 Main Street, East Hartford, CT 06108. Member AIAA.

§Professor, School of Aerospace Engineering. Senior Member AIAA.

I. Introduction

PARTICLE dispersion in wall-bounded flows is important in a number of applications ranging from transport of multiphase mixtures, to friction-drag reduction applications, to environmental studies concerned with the diffusion of contaminants. In aerospace applications, two particular cases of interest are particle ablation, which can occur on high-speed aerodynamic surfaces, and particle erosion, which can occur in solid-propellant rocket engines. In both cases, the gravitational effects are minimal, and turbulence is the primary reason for the particles to spread away from the wall where they were injected. Consistent with the small particle loading for such applications, we consider herein the particle concentration to be dilute, such that particle–particle interactions and the effect of the particles on the surrounding fluid dynamics are negligible. The reasonableness of this assumption will be discussed in terms of the resulting concentration profiles in Sec. III.B.

In general, for a turbulent boundary layer characterized by a fluid kinematic viscosity ν_f, freestream velocity U_∞, and based on a reference location, one can define a friction velocity u_t and a boundary-layer thickness δ. When it is assumed that the particle density is much greater than that of the surrounding fluid, the particle response time τ_p can be related to the terminal velocity V_{term} and the magnitude of the gravitational acceleration g, that is, $\tau_p = V_{\text{term}}/g$. From these values, one can define some key nondimensional parameters that govern turbulent diffusion: the drift parameter γ, outer Stokes number St_δ, inner Stokes number St^+, and wall-shear Reynolds number Re_τ, as follows:

$$\gamma = V_{\text{term}}/u_\tau, \qquad \text{St}_\delta = \tau_p/\tau_\delta = \tau_p/(\delta/u_\tau)$$

$$\text{St}^+ = \tau_p/\tau_f^+ = \tau_p/\left(\nu_f/u_\tau^2\right), \qquad Re_\tau = u_\tau\delta/\nu_f \tag{1}$$

where the subscripts p and f distinguish particle from fluid characteristics, respectively. In the case of homogeneous isotropic stationary turbulence (HIST), particle diffusion is a result of both the crossing trajectory effect (controlled by the drift parameter) and the inertia effect (controlled by the Stokes number). For long-time diffusion ($t \gg \tau_p$ and $t \gg \tau_f$, a relevant fluid timescale) in HIST flows, previous experimental, numerical, and analytical studies have shown that γ is the main parameter (as opposed to Stokes number) in terms of controlling the magnitude of long-time particle diffusion.[1–3]

Particle dispersion in inhomogeneous turbulent flows is significantly more complicated, and, as a result, several aspects of the underlying physics are not well understood. For example, Young and Leeming[4] reviewed particle deposition experiments and noted that the diffusion–impaction regime exhibits a dramatic increase in particle deposition caused by the phenomenon of "turbophoresis" (a convective drift of particles down gradients of mean-square fluctuating velocity). Based on average Eulerian fluid properties and a particle equation of motion, they developed a model for this effect that was shown to agree well with experimentation and that offers improvement over the free-flight theory of Friedlander and Johnstone.[5] McLaughlin[6] and Brooke et al.[7] investigated rigid spherical particles in a vertical channel by using direct numerical simulation (DNS) and found that particles tended to concentrate in the viscous sublayer of the near-wall flow through wallward motions of the turbulence (termed sweep events) in the buffer layer, that is, trapping by coherent streamwise structures. Pedinotti et al.[8] and van Haarlem et al.[9] also used DNS and observed preferential concentration in the low-speed streaks near the channel wall where the effect was most noticeable for intermediate St^+ (on the order of 3–5). Narayanan et al.[10] studied particle dispersion and deposition in the near-wall region of a modified channel flow for $\text{St}^+ = 5$ particles and found that a particle's inertia quickly carries it through the sublayer and onto the wall. Marchioli and Soldati[11] performed particle simulations using DNS and investigated a wide range of Stokes numbers (St^+ of 4–116) and noted that this parameter primarily controlled the turbophoresis phenomenon. Some additional relevant simulations are found in Refs. 12–17 as discussed by Dorgan.[18]

However, none of these DNS studies considered a canonical, spatially growing boundary layer, as is the case for the present research and the experiments of Kaftori et al.[19] A boundary-layer flow includes unique features such as a dramatic dropoff in turbulent kinetic energy and dissipation toward the freestream edge, a mean wall-normal velocity induced by boundary-layer growth, and a continuously developing mean profile. Study of particle dispersion in a turbulent boundary-layer flow is important to several external flowfields, for example, particles ablating from an aerodynamic surface and particles lofted from the ground in an atmospheric boundary layer. The present research is also unique in that it considers a significantly higher Reynolds number (based on channel half-height, pipe radius, or boundary-layer thickness) than the previous multiphase DNS studies just noted. The number of computational nodes was also commensurately large, for example, five times that studied by Narayanan et al.[10]

The particle conditions of the present study are also unique. First, the present research considers a wide range of St^+, from 0.027 to 270. Second, it also considers a fixed and finite drift parameter of 0.01. A finite value of this parameter was used to determine the transition from gravity dominated to inertia dominated conditions for constant γ, but allows exclusive focus on the inertia influence. In particular, a fixed drift parameter will tend to hold the crossing trajectory effect approximately constant and allow focus on inertial effects only. This condition is interesting from a flow physics point of view, but is difficult to investigate experimentally because it requires changing the flow condition, that is, friction velocity, and particle diameter simultaneously. Herein, the gravitational force and particle size could be varied instead to achieve this condition. Third, the present study also considers the injection of particles near the wall (and not distributed throughout the flow as in most of the previous studies) because this injection is consistent with external boundary flows. Fourth, the streamwise recycling of particles often used in channel flows is not employed herein because the flow and, thus, particle concentration, is spatially developing, that is, does not become statistically stationary. Finally, the present research also considers the case of particle reflection, that is, the particles' bounce, when contacting the wall, which is physically consistent for many of the external flows of interest described earlier, but is in contrast to the case in many of the previous studies where particles would stick to the wall.

For these unique flow and particle conditions, we examine particle diffusion, dispersion, reflection, and velocity statistics. This study is for a well-characterized inhomogeneous, anisotropic flow, so that Reynolds-averaged Navier–Stokes-based numerical particle diffusion techniques can be directly evaluated without issues of experimental uncertainties or turbulence model empiricism. (References 18 and 20 contain additional statistics of the flow solution.) In summary, the present research is aimed at isolating and understanding the exclusive effects of inertia on near-wall particle dispersion phenomena for a turbulent boundary layer.

II. Methodology

A. Turbulent Boundary Layer

The continuous-phase solution for the turbulent boundary layer was obtained from a DNS of the incompressible Navier–Stokes equations. The continuous-phase solution is independent of the particle trajectories because the particle concentration is assumed to be dilute and does not effect the carrier phase, that is, the flow only allows one-way coupling of the fluid on the particle motion. The DNS code was developed by Spalart and Watmuff[21] to simulate a three-dimensional, spatially developing boundary layer with zero streamwise pressure gradient. The method is spectrally accurate in the three spatial directions and second-order accurate in time. The solution domain is semi-infinite over a flat, smooth surface with $0 \le x \le L_x$, $0 \le z \le L_z$, and $0 \le y \le \infty$, where x, z, and y represent the streamwise, spanwise, and transverse directions; L_x is the streamwise domain length; and L_z is the length of one period of the periodic spanwise domain. The domain is discretized by 256 nodes in the stream direction, 96 in the span direction, and 55 in the transverse direction, for a total of 1,351,680 nodes in the three-dimensional mesh. To achieve a spatially growing boundary layer, a fringe velocity is included in the momentum transport terms. This decrement effectively subtracts the momentum accumulation due to the spatial growth in the boundary layer. This fringe velocity sources and sinks repose the spatial developing boundary problem as a quasi-periodic problem in the x direction, so that the outflow conditions (suitably modified) are then used as inflow conditions. The useful region of the streamwise domain is defined as the portion of the domain not significantly affected by the fringe boundary conditions and ranges from $x = 0.2L_x$ to $x = 0.8L_x$. Further details are given by Dorgan.[18]

Eulerian time-averaged/spanwise-averaged statistics of the fluid properties at $x = L_x/3$ are shown in Fig. 1 for transverse profiles of the mean velocity ($u^+ = \bar{u}/u_\tau$, where u is the streamwise velocity and u_τ is the reference friction velocity); the turbulent kinetic energy ($k = \frac{1}{2}(\overline{u'_f u'_f} + \overline{v'_f v'_f} + \overline{w'_f w'_f})$ normalized by u_τ); the turbulent

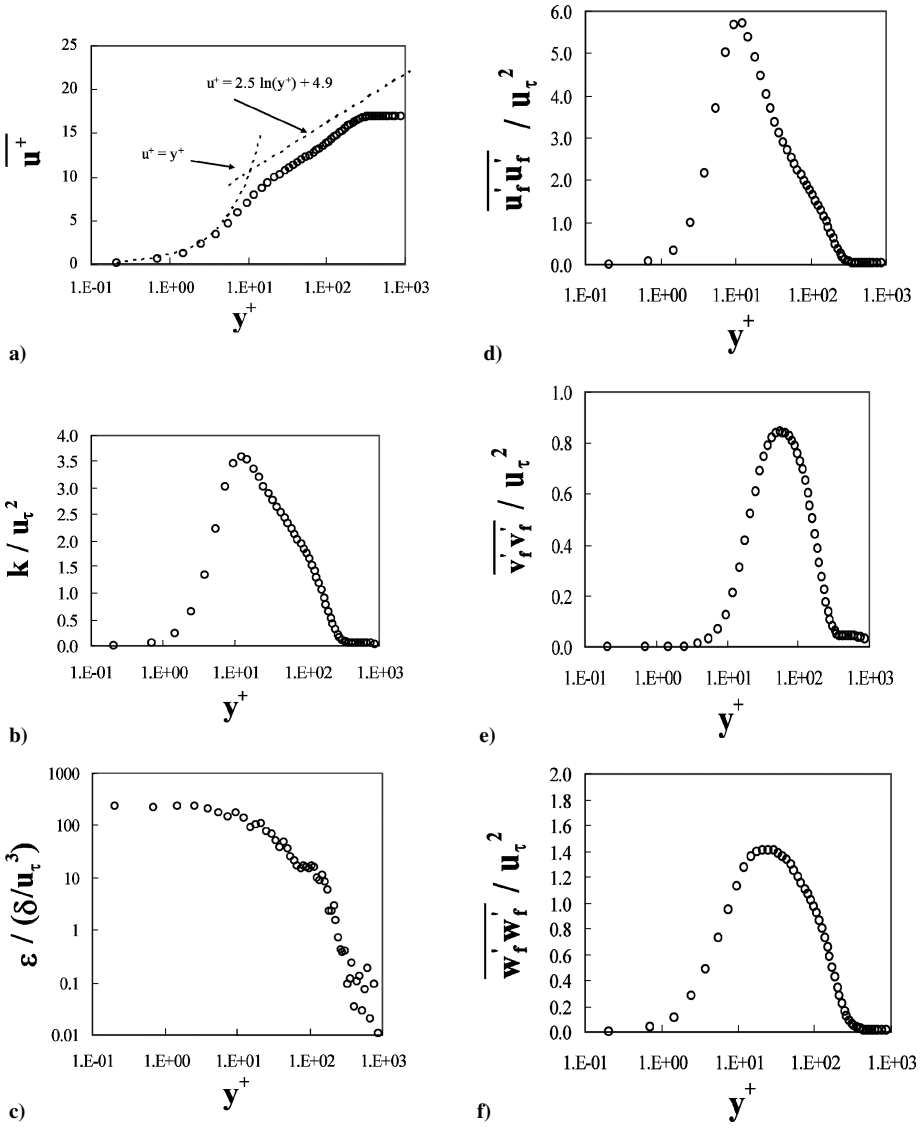

Fig. 1 DNS statistics at $\Lambda_x/3$ for a) mean velocity profile, b) turbulent kinetic energy profile, c) turbulent dissipation per unit mass profile and velocity autocorrelations for the d) streamwise, e) transverse, and f) spanwise fluctuations.

dissipation per unit mass ε, normalized by δ, the reference boundary-layer thickness, and u_τ^3; and the velocity auto-correlations ($\overline{u'_f u'_f}$, $\overline{v'_f v'_f}$, $\overline{w'_f w'_f}$) normalized by u_τ^2. Note that u, v, and w represent the streamwise, vertical, and spanwise velocity components, respectively, and that the same streamwise location was chosen for the reference δ and u_τ values. The Eulerian-averaged properties, denoted as $\bar{q}$ for some arbitrary property q, represent averaging over the spanwise domain and over an integration time period τ_{int} of about 10 τ_δ, and, thus, are a function of (x, y), that is, the Eulerian mean and its perturbation are given by

$$\bar{q}(x, y) = \frac{1}{\tau_{\text{int}}} \int_0^{\tau_{\text{int}}} \left[\frac{1}{\Lambda_z} \int_0^{\Lambda_z} q(x, y, z, t)\, \mathrm{d}z \right] \mathrm{d}t$$

$$q'(x, y, z, t) = q(x, y, z, t) - \bar{q}(x, y) \tag{2}$$

Figure 1a, the profile of the mean streamwise velocity $\overline{u_f}$ at $x = \Lambda_x/3$, normalized by u_τ, shows a viscous sublayer below $y^+ \sim 10$ and a transition to a logarithmic curve by $y^+ \sim 30$. The common law of the wall expressions are included for the purpose of comparing the data to very high-Reynolds-number boundary layers. In Fig. 1b, we note that below $y^+ = 1$ the turbulent kinetic energy is nearly zero and approaches a maximum of about 3.6 at around $y^+ = 15$. Toward the boundary-layer edge, the energy returns to zero, as expected. Figure 1c shows the expected trend for the turbulent dissipation per unit mass for the turbulent boundary layer, albeit with some numerical noise outside the mean boundary-layer edge where the kinetic energy is quite small. Figures 1d–1f give the Eulerian-averaged velocity autocorrelations and show that $u'_f u'_f$ is the largest of the three autocorrelations, peaking at nearly $6u_\tau$ very close to the wall at a y^+ of around 10. The transverse velocity fluctuations represent the smallest autocorrelation and peaks furthest away from the wall, such that the peak magnitude of $v'_f v'_f$ is only $0.9u_\tau$ at y^+ of about 70. Note that the turbulence intensity (rms) in the three directions is defined from the autocorrelations, for example, $v'_{f,\text{rms}}(x, y) = [\overline{v'_f v'_f}(x, y)]^{1/2}$. These kinetic energy and velocity fluctuation results are similar in magnitude to the experimental results of Klebanov reported by Hinze (see Ref. 22) at $Re_\tau = 2800$.

To better characterize the turbulence timescale of the fluid, an integral Lagrangian timescale τ_Λ can be defined based on the Lagrangian decorrelation of the streamwise velocity fluctuations. This is based on an ensemble average from the release of many fluid tracers (particles that have no inertia and, thus, move at the speed of the fluid velocity) injected over the full spanwise range ($z_0 = [0, L_z]$) and released at various instances throughout a long time period ($t_0 = [0, \tau_{\text{int}} - \tau_{\text{dom}}]$), where τ_{dom} is the average time for a fluid tracer to traverse the interrogation domain (15 boundary-layer thicknesses)

and where the subscript zero denotes the injection conditions. These fluid tracers were released at the reference plane $x_0 = L_x/3$ and at various y_0 stations (from near to the wall to well above the boundary layer). The velocity correlations were then tracked over fluid Lagrangian paths and integrated to obtain the decorrelation timescale for each fluid tracer. This result was then averaged over all fluid tracers released at a transverse location. The Lagrangian integral timescale for the streamwise velocity fluctuations is, therefore,

$$\tau_{u'_f,\Lambda}(y_0) = \left(\frac{1}{F}\right)\sum_{i=1}^{F} \times \frac{\int_{t_0}^{t_1} u'_f(x_0, y_0, z_0, t_0)u'_f(x_0 + \Delta x_f, y_0 + \Delta y_f, z_0 + \Delta z_f, t)\,\mathrm{d}t}{[1/(t_1 - t_0)]\int_{t_0}^{t_1} u'_f(x_0, y_0, z_0, t_0)u'_f(x_0, y_0, z_0, t_0)\,\mathrm{d}t} \tag{3}$$

where

$$\Delta x_f(t) = \int_{t_0}^{t} u_f(x, y, z, \tau)\,\mathrm{d}\tau, \qquad \Delta y_f(t) = \int_{t_0}^{t} v_f(x, y, z, \tau)\,\mathrm{d}\tau$$

$$\Delta z_f(t) = \int_{t_0}^{t} w_f(x, y, z, \tau)\,\mathrm{d}\tau$$

and where F is the total number of fluid tracers released at a given y_0 station. Similarly, $\tau_{v'_f,\Lambda}$ and $\tau_{w'_f,\Lambda}$ were obtained, and the three timescales were linearly averaged together to give τ_Λ as a function of y_0 (Ref. 20). This timescale is used as an approximation of the turbulence local lifetime, though weak changes can be expected as a function of streamwise location.

B. Particle Equation of Motion and Statistics

The Lagrangian equation of motion for a rigid particle used herein is given by

$$m_p \frac{\mathrm{d}\boldsymbol{V}_p}{\mathrm{d}t} = \boldsymbol{F}_D + \boldsymbol{F}_G \tag{4}$$

where m_p is the particle mass, $\boldsymbol{F}_D$ is the steady-state drag force, $\boldsymbol{F}_G$ is the buoyancy force, and $\boldsymbol{V}_p$ is the particle velocity vector. The particle density was assumed to be much greater than the fluid density, such that virtual mass and secondary forces due to lift, fluid stress gradient, and particle history can be assumed negligible. Note that the neglect of lift may be the most important approximation because the particles will often be located in the high-shear near-wall region. The particle hydrodynamic forces for this study are summarized as

$$\boldsymbol{F}_D = -\tfrac{1}{2}\rho_f |\boldsymbol{V}_{\mathrm{rel}}|\boldsymbol{V}_{\mathrm{rel}}\pi\left(d_p^2/4\right)C_D, \qquad F_{G_i} = m_p g_i \tag{5}$$

where $\boldsymbol{V}_{\mathrm{rel}}(=\boldsymbol{V}_p - \boldsymbol{V}_f)$ is the magnitude of the relative velocity vector, which is equal to $\boldsymbol{V}_{\mathrm{term}}$ in quiescent conditions. A Stokesian drag law ($C_D = 24/Re_p$, where $Re_p = d_p|\boldsymbol{V}_{\mathrm{rel}}|/\nu_f$) has been employed because it allows understanding of the fluid physics without introducing the nonlinearities and empiricism associated with high Reynolds number expressions. From this, the particle response time can be written in terms of the particle mass as $\tau_p = m_p/18\mathrm{d}\rho_f\nu_f$.

The particle trajectories are computed by numerically integrating the particle equation of motion using the exponential Lagrangian method as described by Barton[23] and as modified by Bocksell[20] to include gravitational effects:

$$V_p(t + \Delta t) = V_p(t)\exp(-\Delta t/\tau_p) + [1 - \exp(-\Delta t/\tau_p)][(1/\tau_p)V_f(t) + g]\tau_p \tag{6}$$

This scheme was implemented in an Adams–Bashforth, predictor–corrector fashion for second-order accuracy in time. The number of particles used in each simulation was varied over a significant range to ensure statistical convergence for all results presented herein. In the computation of the statistical average along the particle trajectory, interpolation between the computational nodes to the particle location is required. This was accomplished by using the surrounding eight fluid nodes as corner points for trilinear interpolation of the fluid velocity. Because of the fine grid resolution, this was found to be sufficiently accurate for all of the statistical results presented herein, such that a spectrally accurate interpolation was not needed.

C. Test Conditions

The baseline test condition for the particle/turbulent boundary-layer interaction was chosen as $\mathrm{St}_\delta = 10^{-2}$ and $\gamma = 10^{-2}$. This represents a relatively rapid, but finite, response of the particle to the large-scale turbulent structures, for example, it corresponds, hypothetically, to a 24-μm-diam solid sphere with a density of 1000 kg/m^3 in a flow of air with $\delta = 22$ cm and $u_\tau = 1.47$ m/s (Reynolds number of approximately 2.2×10^4). In this case, the particle radius is equal to one wall unit, that is, contact with the wall occurs when the transverse location of the particle centroid y_p^+ equals one (a boundary condition to be employed herein).

To vary the particle inertia, the general test conditions used a range of five outer Stokes numbers St_δ equally spaced on a logarithmic scale from 10^{-4} to 10^0, all for a constant γ of 10^{-2}. For this small γ, inertia and turbulent diffusion effects will dominate the particle dispersion (as opposed to gravity) to be in line with the objectives of this study. One of the statistics to be gathered is the Lagrangian average along the particle path, that is,

$$\langle q \rangle = \left[\frac{1}{N}\right]\sum_{i=1}^{N} \frac{1}{(t_1 - t_0)}\int_{t_0}^{t_1} q(x_0 + \Delta x_p, y_0 + \Delta y_p, z_0 + \Delta z_p, t)\,\mathrm{d}t \tag{7}$$

where

$$\Delta x_p(t) = \int_{t_0}^{t} u_p(x, y, z, \tau)\,\mathrm{d}\tau, \qquad \Delta y_p(t) = \int_{t_0}^{t} v_p(x, y, z, \tau)\,\mathrm{d}\tau$$

$$\Delta z_p(t) = \int_{t_0}^{t} w_p(x, y, z, \tau)\,\mathrm{d}\tau$$

where N is the total number of particles injected (all injected at $y_0^+ = 4$ and $x_0 = L_x/3$). From this definition, the average local Lagrangian particle Stokes number can be obtained as

$$\langle \mathrm{St}_\Lambda \rangle = \tau_p/\langle \tau_\Lambda(y_p) \rangle \tag{8}$$

for a given class of particles, and is bounded (as expected) by St^+ and St_δ as shown in Table 1. Recall that St_δ and St^+ are based on the flow parameters at the injection location only and, thus, are only qualitative estimates for the particle characteristics throughout the domain, whereas $\langle \mathrm{St}_\Lambda \rangle$ is based on an average integrated along particle paths throughout the domain. Note that the domain time (τ_{dom}, the average time required for a particle to traverse the tracking domain) is relatively large compared to the particle response times and integral timescales. Note also that the conditions are not universal in that changes in the boundary-layer Reynolds number will alter

Table 1 Particle test conditions with various Stokes numbers and integration times

St_δ	$\langle \mathrm{St}_\Lambda \rangle$	St^+	$\tau_{\mathrm{dom}}/\tau_\Lambda$	$\tau_{\mathrm{dom}}/\tau_p$
1.0E−04	7.8E−04	2.7E−02	12.6	1.6E+04
1.0E−03	7.8E−03	2.7E−01	12.7	1.6E+03
1.0E−02	8.3E−02	2.7E+00	14.6	1.8E+02
1.0E−01	1.2E+00	2.7E+01	30.7	2.6E+01
1.0E+00	1.4E+01	2.7E+02	45.6	3.3E+00

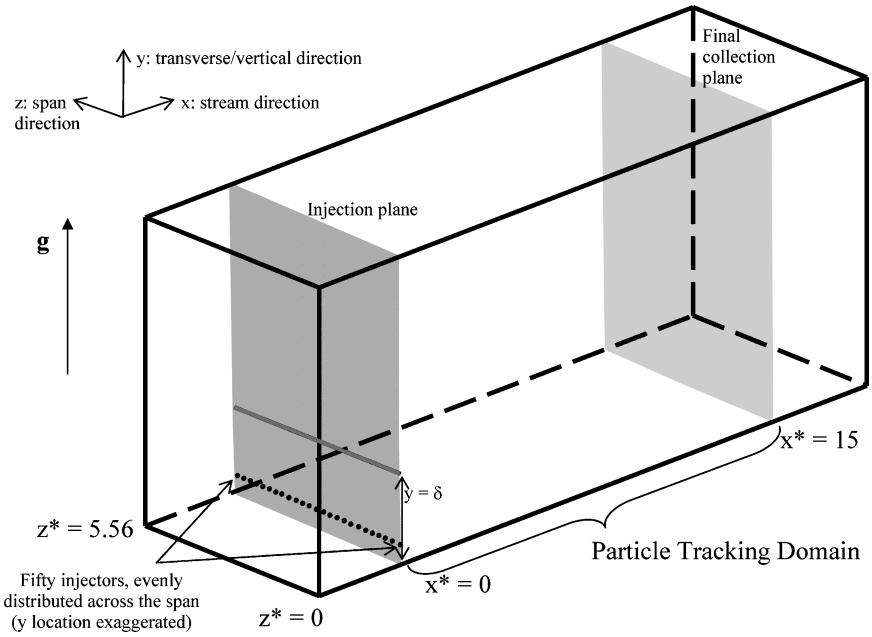

Fig. 2 Schematic of particle injection location (x_0, y_0, z_0) and particle tracking domain; gravity and terminal velocity of particles directed in y direction, away from wall.

the ratio between the inner and outer timescales; however, it is expected that the behavior and statistics of particles in the near-wall region will tend to scale with St^+, whereas particle results in the outer region will tend to scale with St_δ. In addition, δ and u_τ will change within the test area because the boundary layer is spatially developing and will result in small changes in these Stokes numbers if defined at other streamwise locations. (Note that this problem does not occur with constant channel flow simulations.) However, St_Λ does not suffer from this problem because it was obtained as an average throughout this domain.

The particles were injected at uniform spanwise locations at $y_0^+ = 4$ and $x_0 = L_x/3$ and tracked through a distance of 15 boundary-layer thicknesses downstream (Fig. 2). This streamwise injection location corresponds to $Re_\delta = 4500$ (based on U_∞ and δ) and $Re_\tau \approx 270$ (based on u_τ and δ). There were 50 particles injected every other time step, that is, at every $0.57\tau_f^+$, for a period of 4000 time steps (4.38 τ_δ) such that a total of 100,000 particles were injected (a large enough group for converged statistical results). A typical simulation lasted around 12,000 time steps and took approximately 21 wall clock hours of compute time on a single processor. The streamwise portion of the particle tracking region was nondimensionalized with respect to the reference boundary-layer thickness as $0 \le x^* \le 15$, where $x^* = (x - L_x/3)/\delta$, and the reference boundary-layer thickness δ is the thickness at $L_x/3$. Similarly, the spanwise domain was nondimensionalized by δ to obtain $0 \le z^* \le 5.56$, where $z^* = L_z/\delta$.

The particles were injected with the sum of the mean fluid velocity and the terminal velocity, that is, with $u_p = \overline{u_f}$ (approximately $4u_\tau$), $v_p = \overline{v_f} + V_{\text{term}}$, and $w_p = \overline{w_f} = 0$. This choice of injection (as opposed to injecting at the instantaneous fluid velocity plus the terminal velocity) ensured that the particles with the largest Stokes numbers would not possess unrealistically large initial velocity variations that are generally inconsistent with their long response times. Note that the choice of the initial velocity for the small particles is not as important because the initial conditions will be more quickly forgotten due to faster response times.

To prevent wall collisions from acting as the dominant dispersion phenomena for the larger particles, the particle's terminal velocity is directed away from the wall, consistent with ablation from a lower aerodynamic surface, and a perfectly elastic wall collision at y^+ of one was imposed as a reflection condition (consistent with the hypothetical physical particle dimensions).

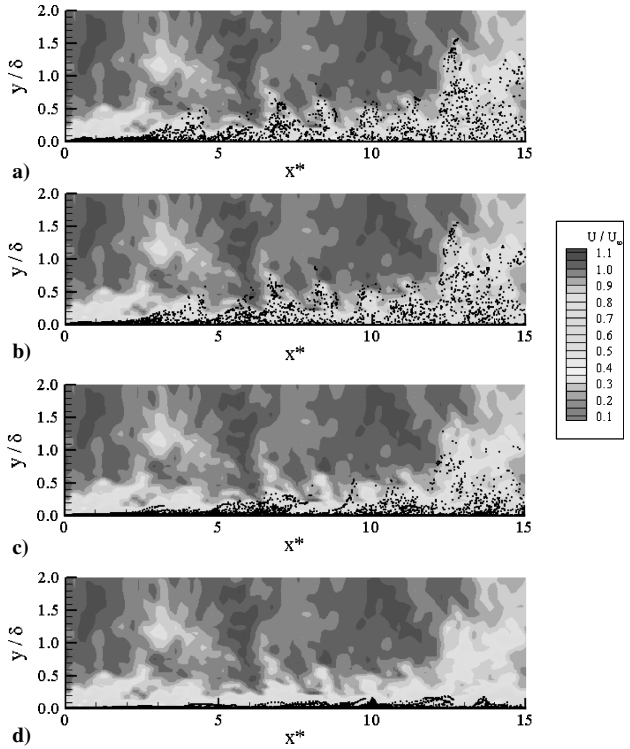

Fig. 3 Instantaneous fluid solution at $z^* = 2.78$ with particle locations: a) $St_\delta = 10^{-4}$ ($St^+ = 0.027$), b) $St_\delta = 10^{-2}$ ($St^+ = 2.7$), c) $St_\delta = 10^{-1}$ ($St^+ = 27$), and d) $St_\delta = 10^0$ ($St^+ = 270$).

III. Results

A. Particle Dispersion Structures

To investigate preferential concentration as observed in previous studies with channel flow, the particle positions were mapped onto the streamwise velocity field. Figures 3 and 4 show the instantaneous fluid solution and particle locations for the $St_\delta = 10^{-4}$, 10^{-2}, 10^{-1}, and 10^0 cases for $z^* = 2.78$ (vertical plane) and $y^+ = 9.66$ (a horizontal plane). In Figs. 3a and 3b (both with $St^+ < 1$ and $St_\delta \ll 1$), the particles injected at $x^* = 0$ can be seen to diffuse away from the

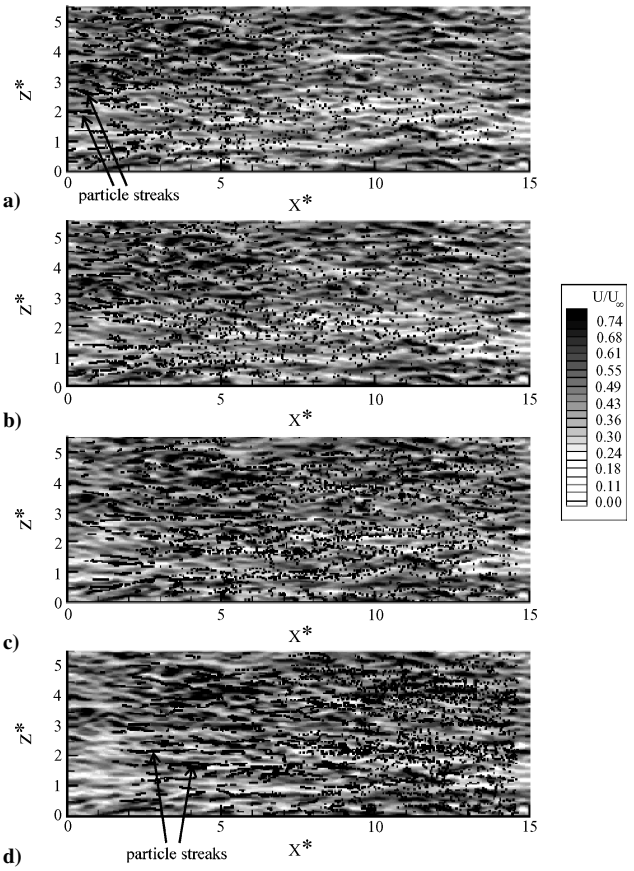

Fig. 4 Instantaneous fluid solution at $y^+ = 9.66$ (where $\overline{u_f} = 0.42$) with particle locations a) $St_\delta = 10^{-4}$ ($St^+ = 0.027$), b) $St_\delta = 10^{-2}$ ($St^+ = 2.7$), c) $St_\delta = 10^{-1}$ ($St^+ = 27$), and d) $St_\delta = 10^{0}$ ($St^+ = 270$).

wall, primarily via low-speed fluid ejections, and are nearly diffused as a fluid tracer. These particle ejections tend to have vertical scales and streamwise separations of about one δ. As inertia increases (to $St^+ = 2.7$ and 27 in Figs. 3c and 3d) the particle diffusion away from the wall is substantially delayed (spatially), and the particles are more likely to be located along the wall, though the streamwise separations are still about one δ in scale. These near-wall injection results (whereby diffusion is primarily away from the wall) are much different than previous channel flow results with uniformly distributed particle injection (where turbulent diffusion generally leads to a net movement toward the wall). However, one study that considered near-wall injection conditions was that of Soltani and Ahmadi,[24] who observed qualitatively similar behavior as found herein.

To see the spanwise structure, particles are considered along a near-wall horizontal plane in Fig. 4. The Eulerian mean velocity $\overline{u_f}$ at this y location is 0.42 and is depicted with gray contours. The particles (shown as black dots) are located above and below the fluid plane in a region extending from $7.44 < y^+ < 12.2$. This transverse range was chosen to be large enough to include several particle positions, yet sufficiently small to ensure that the selected fluid plane is a good representation of the fluid solution over the transverse range and, thus, at the actual particle location. Toward the left of each of Figs. 4 ($x^* < 3$ for $St_\delta = 10^{-4}$ and $x^* < 9$ for $St_\delta = 10^0$), there are very compact streaks of particles (indicated by black arrows in Figs. 4a and 4d). These particles are moving up from the injection location at $y^+ = 4$ into the collection bin, whose floor is set to 7.44 inner units. The lowest inertia ($St^+ = 0.027$) particles (which behave nearly as fluid tracers) initially move upward with the fluid and are generally located in low-speed streaks because $\overline{u'_f v'_f}$ is negative for the boundary layer. After moving sufficiently downstream ($x^* > 3$), the particle trajectories lose memory of the initial ejections, and the correlation of particle location with low-speed streaks is lost (as expected).

At an $St_\delta = 10^{-2}$, the particle streaks are reduced in intensity downstream as the local concentration is reduced. However, there is a continued correlation of particles in low-speed streaks (white), or, equivalently, an absence of particles in (black) high-speed streaks. At this flow condition ($St^+ = 2.7$), the correlation (preferential concentration) appears to be stronger than at any of the other St^+ values. This is consistent with the channel flow results of Pedinotti et al.[8] and Marchioli and Soldati.[11] This correlation is also noticeable at a Stokes number of $St_\delta = 10^{-1}$ (which corresponds to $St_\Lambda = 1.2$ and $St^+ = 27$), however, it is more focused in the longer low-speed streaks, whereas some particles can be seen in the small-scale high-speed regions. In the highest Stokes number case ($St_\delta = 10^0$), the particles move up in the same streaky fashion, but do not necessarily correspond to low-speed streaks at this entry point because their inertia is sufficiently large to allow them to be unresponsive to the small-scale structures. Thus, their initial streaks are primarily a consequence of the initial conditions imposed on the particle. Farther downstream, as the effect of the initial conditions subsides, the particles tend to preferentially concentrate themselves in only the longest (long timescale) low-speed streaks, located in the bottom right half of Fig. 4, while remaining uncorrelated with the small-scale structures; that is, they are just as likely to be observed in small high-speed regions as they are in small low-speed regions. These results are qualitatively similar to those by Marchioli and Soldati[11] and van Haarlem et al.,[9] but those results show streaks that are much more compact in the spanwise direction and much longer in the streamwise direction, which may be due the present wall reflection condition that effectively produces specular diffusion near the wall.

B. Particle Diffusion Behavior

Transverse particle distributions are shown in Fig. 5 for various particle sizes, where C represents the ensemble average of the mean Eulerian concentration of particles (obtained through net flux statistics) and C_0 is the bulk concentration fluxing through the reference boundary-layer thickness. Figures 5a and 5b show the particle transverse distribution profile at 8 and 15 boundary-layer thicknesses downstream of the injection location; the y^+ data points are at the center of each of the 26 transverse bins. In Fig. 5a ($x^* = 8$), the smallest two particles ($St_\delta = 10^{-4}$ and 10^{-3}) yield nearly the same results. This is consistent with their condition of $St^+ < 1$ so that they effectively act as tracers and are primarily governed by fluid turbulent mixing. As a result, they quickly diffuse away from the wall, such that the overall particle distribution extends significantly beyond y^+ of 100, that is, beyond y/δ of 0.4, where one expects that particle diffusion is dominated by large-scale structures and St_δ.

The larger $St_\delta = 10^{-2}$ particles begin to show the influence of inertia. Whereas the outer portion of the profile ($y^+ > 30$) is nearly identical to the profiles for the smaller particles, there is a higher concentration of particles in the near-wall region ($y^+ < 10$). These two results are expected because the outer region should be governed by St_δ (which is still much less than one, such that these particles should act similar to a passive scalar), whereas the near-wall region should be governed by St^+ (which is of order one for this particle condition and, therefore, should demonstrate inertial tendencies in the near-wall region). Note that the increased near-wall concentration is not expected to be a result of reduced mean diffusion due to particle size increases in homogeneous turbulence because such diffusion rate reductions are due to increases in γ, from the crossing trajectory effect, which is fixed in the current simulations. Therefore, the concentration increase is due to inhomogeneous turbulence, as discussed by Young and Leeming,[4] whereby particles move away from high-turbulence regions and, thus, avoid moving toward the turbulence peak, that is, avoid moving away from the wall.

The remaining two cases ($St_\delta = 10^{-1}$ and 10^0) also have peak concentrations below y^+ of 10, but with much higher values. This is consistent with the model of Young and Leeming,[4] for which such wall Stokes numbers ($St^+ = 27$ and 270) correspond to the highest turbophoretic velocities toward the wall. Thus, nonhomogeneous turbulence aspects play a strong role in the reduced diffusion of very large St^+ particles in spatially developing boundary layers with reflective wall conditions. This result is very similar to the flux distribution observed for St^+ ranging from 0.6 to 14 in the boundary-layer experiments of Kaftori et al.,[19] shown in their Fig. 12, for

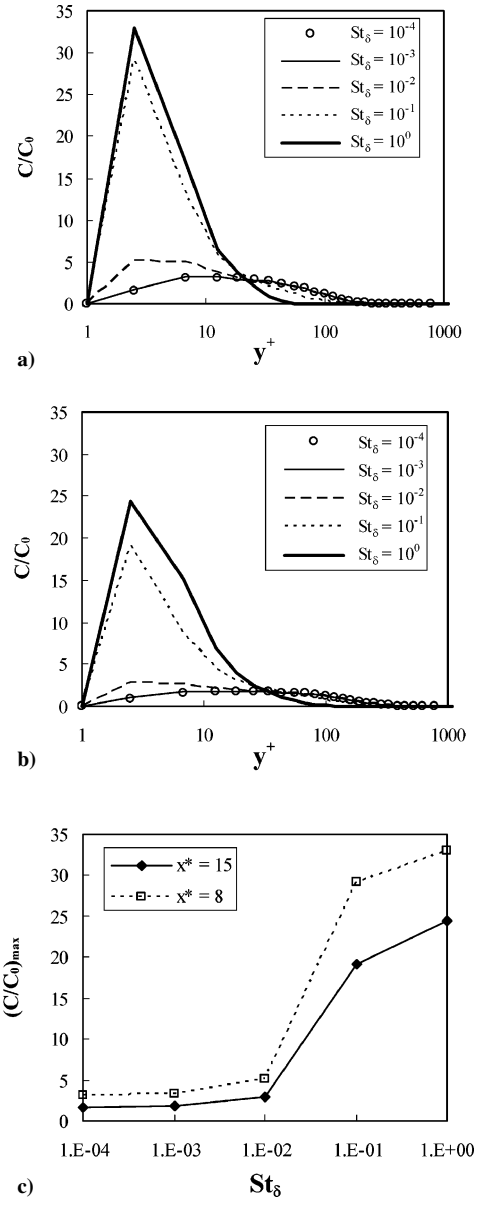

Fig. 5 Particle concentration: a) transverse profiles for $x^* = 8$, b) transverse profiles for $x^* = 15$, and c) maximum particle concentration as a function of outer Stokes number.

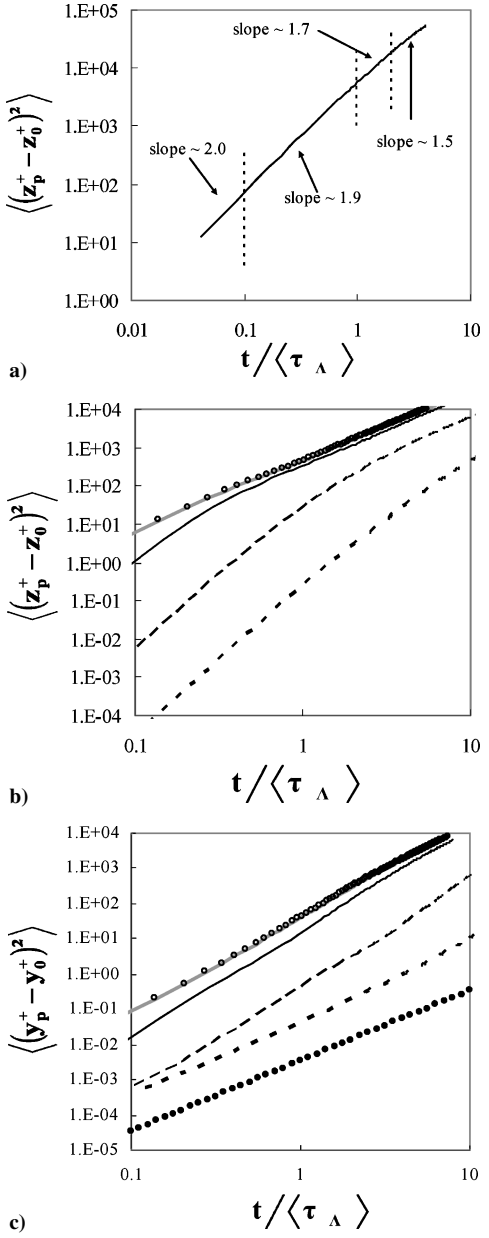

Fig. 6 Mean-square deviation from the injection location in a) spanwise direction for an approximate fluid tracer injected at $y^+ = 100$, b) spanwise direction for DNS test matrix, and c) transverse direction for DNS test matrix: ○, $St_\delta = 10^{-4}$; ——, $St_\delta = 10^{-3}$; ——, $St_\delta = 10^{-2}$; - - - -, $St_\delta = 10^{-1}$; – – –, $St_\delta = 10^{0}$; and ●, tV_{term}.

which elastic wall rebound may be expected. Note that the present reflection boundary condition at $y^+ = 1$ results in a different concentration profile than previous, nonreflecting channel flow results, for example, those of Narayanan et al.[10] and van Haarlem et al.,[9] which yield a continued particle concentration increase toward $y^+ = 0$.

Figure 5b shows the concentration profile for the last collection plane located at 15 boundary-layer thicknesses downstream of the injection location. In general, the same trends discussed earlier can be seen, but with differences due to the convection and diffusion farther downstream. In particular, there is a decay of the peak concentration or, equivalently, a broadening of the profile for all cases. Note that the net shift in the peak concentration away from the wall due to the imposed terminal velocity on the particle trajectories does not play a major role in the concentration profiles because it is small. (It corresponds to a Δy^+ of about one, which is small compared to the bin resolution.) As expected, the decay of the peak concentration for $St_\delta = 1$ is somewhat slower than for $St_\delta = 10^{-1}$, and is attributed to the increased (10 times larger) inertia.

Figure 5c quantifies the change in the peak concentration for the range of Stokes numbers investigated. The peak concentration increases with Stokes number for high inertias (due to the lack of long-time behavior) and decays nearly linearly with x/δ; that is, a twofold increase in x corresponds, roughly, to a twofold decrease in C_{max}. This will be found to be consistent with the results in Fig. 6, where the diffusion rates will be quantified.

Near the injection location ($x/\delta = 0.5$), the particle concentrations for all cases were on the order of 25–35 times the bulk concentration C_0; that is, about one-half of the particles were concentrated at a y^+ of 10 or less. Whereas these high concentration levels generally decreased with distance from the injection location,[20] the high Stokes number particles give concentrations levels of 20–30 times the bulk concentration even far downstream of the initial injection. Thus, the dilute flow assumption should be considered (at least) in terms of the local mean concentrations based on C, which can be very high near the wall. One way to estimate whether a flow is dilute is to estimate the momentum coupling parameter, which is the ratio of momentum flux of the continuous-phase flow to the net force applied to the fluid by the particles. To quantify the momentum coupling parameter for the peak concentrations described earlier (assuming a mean continuous-fluid velocity of $5u_\tau$ and terminal

velocity of 0.01 u_τ), the coupling parameter is approximately 10^{-2}, indicating that the effect of the particles on the mean momentum is small. However, a coupling parameter defined instead on the mean turbulent kinetic energy through this flux surface will be on the order of 10^{-1}, indicating that the turbulence may be significantly affected, especially in local regions, because preferential concentration can cause increased concentrations in streaks as, for example, in Fig. 4b. Thus, the present results should only be considered in terms of a low-concentration limit. Note that simulations with fewer total particles were also completed and gave similar results in terms of mean concentration profiles, etc.

Another issue that should be considered when interpreting the present results is that neglecting lift (as is assumed herein) may not always be appropriate. If one assumes a nonrotating particle in the laminar sublayer (where the mean shear is the highest and on the order of u_τ/d), the ratio of Saffman lift to Stokes drag is on the order of 10^{-1}. Particle rotation can significantly reduce this ratio (by an order of magnitude), such that the mean lift is not expected to be substantial. However, instantaneous lift can be important (especially with respect to turbulent diffusion) because fluctuations in vorticity are significantly higher than the mean vorticity. Thus, the present results are only important when drag dominates the particle surface forces.

Before examination of the particle diffusion rates for near-wall injection, a preliminary test was completed with a group of $\mathrm{St}_\delta = \gamma = 10^{-4}$ particles (essentially fluid tracers), released at $y^+ = 100$ (where the boundary layer should be approximately homogeneous and isotropic). The spanwise diffusion statistics of the particle cloud are shown in Fig. 6a, where the temporal variation is normalized by $\langle \tau_\Lambda \rangle$, the mean integral fluid timescale along the particle path. This timescale was chosen as the normalizing parameter because it allows a clear identification of short-time behavior ($t \ll \langle \tau_\Lambda \rangle$) and long-time behavior ($t \gg \langle \tau_\Lambda \rangle$ and $t \gg \tau_p$, where the latter condition is always satisfied for these nearly tracer particles). The resulting diffusion curve is broken into four pieces, and the slope of each piece is estimated. For normalized times less than 0.1, the slope of the diffusion curve is approximately two, consistent with the short-time particle diffusion rates in HIST.[16] At longer times, a decreasing slope is seen where it is expected that the slope would approach unity for $t/\langle \tau_\Lambda \rangle \gg 30$, which is consistent with the linear long-time particle diffusion in HIST.[22] Thus, particle diffusion away from the wall tends to obey a conventional transition from short-time to long-time diffusion associated with homogeneous isotropic stationary turbulence.

Figures 6b and 6c show the mean-square particle deviation from the injection location in the spanwise and vertical directions, respectively. The timescale (the time elapsed since a particle's injection) is again normalized by $\langle \tau_\Lambda \rangle$. The maximum time used in these statistics was based on a period in which all particles could be tracked within the useful region of the flow domain. (This avoids bias associated with slower moving particles that would tend to stay in the computational domain for longer times.)

First, the mean-square spanwise deviation from the near-wall injection location is considered (Fig. 6b). Because there is no component of terminal velocity or turbulence gradient in the spanwise direction (and, thus, no mean spanwise drift), this statistic can be directly related to the turbulent particle diffusion. The two smallest particle conditions ($\mathrm{St}_\delta = 10^{-4}$ and 10^{-3}) give the highest amount of diffusion and nearly identical results. However, it is interesting that they display an approximately quadratic diffusion rate even for times on the order of $10\langle \tau_\Lambda \rangle$. This is attributed to continued movement of the mean particle location to transverse locations of higher transverse velocity fluctuations (Fig. 1c).

Compared to the smallest particle cases, the higher Stokes number particle clouds are initially hindered by their inertia in diffusing in the spanwise direction, but later diffuse at higher rates (superquadratic for $\mathrm{St}_\delta = 1$). This is attributed to the fact that the largest particles remain much closer to the wall than in the $\mathrm{St}_\delta = 10^{-3}$ and 10^{-4} cases. This near-wall proximity and high inertia initially prevents a large amount of diffusion away from the wall until the integration time becomes sufficiently large, at which point movement away from the wall takes the particles to regions of rapidly increasing spanwise fluid velocity fluctuations.

With respect to the transverse diffusion of Fig. 6c, note that a small portion of the increase in $(y^+ - y_0^+)$ is associated with the terminal velocity rise ($= t V_{\mathrm{term}}$). This portion is shown with the circle symbols and corresponds to quadratic increases in $(y^+ - y_0^+)^2$. The effect is most noticeable for the largest particles because their high inertia results in a relatively small amount of transverse turbulent diffusion. Whereas this terminal velocity influence does exist for all particles, its effect is negligible in the smallest inertia condition where the particles are dominated by asymmetric (away from the wall) turbulent diffusion. Again, we note that the 10^{-3} and 10^{-4} St_δ cases are nearly identical because they behave approximately as fluid tracers (because their St^+ is less than unity). Additionally, it is observed that the asymmetric turbulence yields diffusion rates that are superquadratic (whereas comparable homogeneous diffusion rates were subquadratic after similar integration times). This is attributed to particle movement into regions of higher transverse velocity fluctuations, which do not peak until y^+ of about 70 (Fig. 1c). Thus, the nonlinear diffusion rates are a consequence of the near-wall injection test conditions.

C. Particle–Wall Collisions

Figure 7a shows the nondimensional spatial frequency of wall-collisions (f_{bounce}) for several Stokes numbers vs x^* locations. The wall collision spatial frequency is defined as the average number of particle bounces per unit distance and was obtained by normalizing the total number of bounces in a particular streamwise bin by the length of that bin and the total number of particles N. For all of the particles considered, the number of collisions initially increases with x^* until a peak is reached that is dependent on St^+. Beyond this peak location, the number of collisions decreases as a result of the particle cloud becoming more diffused. As discussed earlier, the 10^{-4} case behaves nearly as a fluid tracer, that is, it moves like a Lagrangian fluid particle, and is, thus, included as a reference. For these particles, the reflection condition imposed at $y^+ = 1$ and the nonequilibrium initial condition yields a finite number of bounces at the initial locations, but this tends to be insignificant downstream. Very little difference is noted between the $\mathrm{St}_\delta = 10^{-4}$ case and the $\mathrm{St}_\delta = 10^{-3}$ (not shown) and $\mathrm{St}_\delta = 10^{-2}$ cases ($\mathrm{St}^+ = 2.7$), indicating the same spatial frequency due to the reflection condition. A dramatic increase in bouncing is noted for the largest two particles ($\mathrm{St}_\delta = 10^{-1}$ and 10^0) because their response time is too large to react effectively to the retardation of the fluid velocity as the wall is approached: They tend to crash through the slower moving fluid. The $\mathrm{St}_\delta = 10^{-1}$ particle initially has many more bounces than the larger 10^0 particle and is attributed to the latter's extremely large inertia. By the last collection bin, the two particles conditions are seen to behave almost identically (a result that is discussed further in the following text). Figure 7b shows the spatial bouncing frequency at the furthest downstream location ($x^* = 15$) where an approximate equilibrium is approached.

The nondimensional deposition rate V_{dep}^+ for the present results was estimated by basing the total time over which the wall collisions occurred on the average particle streamwise velocity, the length of the bounce bin considered (corresponding to 7δ for the last bin), and the time necessary to inject the total number of particles. As shown in Fig. 7c, despite the differences between the present conditions (a boundary layer with constant γ and with near-wall injections coupled with elastic reflections) and those of previous studies (pipe and channel flow configurations with variable γ and with initially uniform particle distribution coupled with nonreflecting conditions), the results are similar for $\mathrm{St}^+ > 1$. This confirms that the bouncing frequencies in the present flow conditions are primarily controlled by St^+ (and not γ). Note that the present deposition velocity tended to plateau at $\mathrm{St}^+ < 1$ due to the reflection condition at $y^+ = 1$, which is different than in previous studies with nonreflecting conditions.

Figures 8a and 8b show the horizontal and vertical wall impact velocities normalized by u_τ for wall collisions occurring between 7 and 15 boundary-layer thicknesses downstream of injection. This

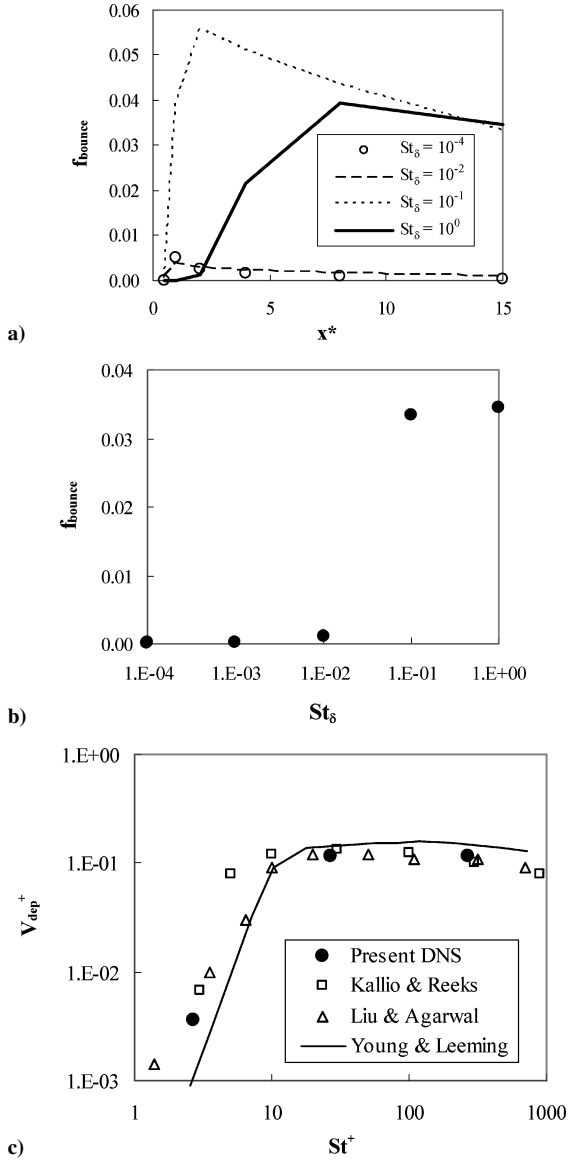

Fig. 7 Nondimensional spatial boucing frequency as a function of a) streamwise distance, b) St_δ, and c) St^+ in terms of equivalent depositional velocity; results in parts b and c averaged over surface given by $7 \le x^* \le 15$.

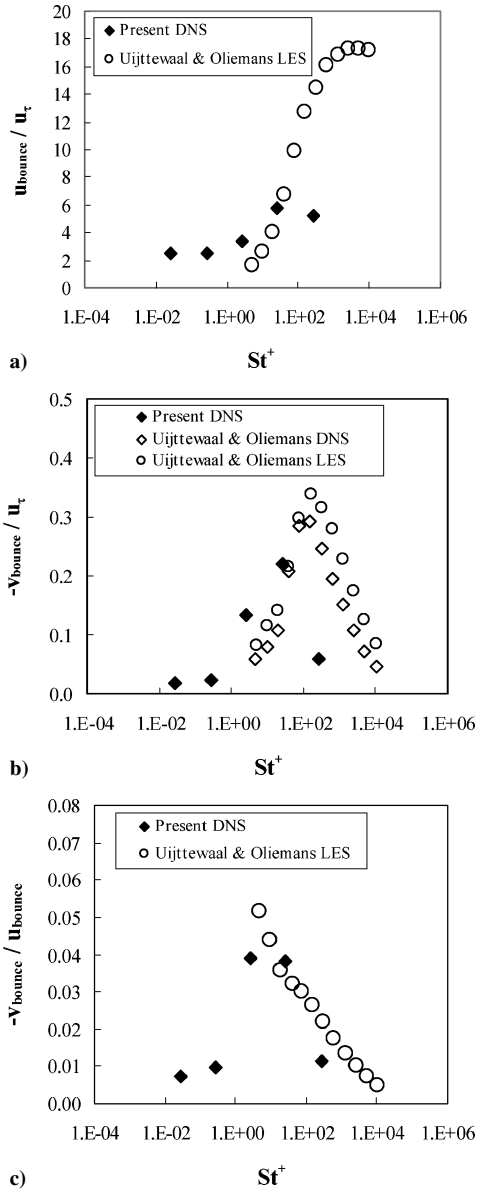

Fig. 8 Bounce impact velocity statistics: a) horizontal component, b) vertical component, and c) ratio of components.

particular streamwise range was chosen to minimize the effect of the particle's injection condition on statistics. Similar to the results of Uijttewaal and Oliemans,[25] the magnitude of the particle's horizontal and vertical impact velocities were found generally to scale more with u_τ than V_{term} because the present terminal velocity acts away from the wall, and the wall collisions are caused by the fluid turbulence. The streamwise velocity on particle impact (Fig. 8a) is on the order of a few u_τ, which is consistent with the local continuous-phase fluid velocities. For example, the largest inertia particles tend to be concentrated at a y^+ of approximately 3–6 (as noted in Fig. 5) and to have impact streamwise velocities consistent with the continuous fluid velocities from that region, that is, $u_{\text{bounce}} \sim 4$–$5u_\tau$, because they cannot appreciably slow down before impacting the wall. The Uijttewaal and Oliemans[25] study reported much higher streamwise impact velocities, which is attributed to their particles being injected far above the inner layer and, thus, having emanated from higher-speed regions before being swept to toward the wall. The decrease in this velocity for the smaller inertias ($St^+ < 10$) is a result of their quicker response times, such that the particles' streamwise velocities are reduced as they move toward the wall and into lower-speed fluid. For these particles, the reflection at $y^+ = 1$ results in a u^+_{bounce} of about $2u_\tau$, whereas the smallest particle reported by Uijttewaal and Oliemans[25] did not interact with the wall until $y^+ = 0.15$ and, thus, can be slowed even further.

The magnitude of the vertical impact velocity is shown in Fig. 8b. The smallest two cases ($St_\delta = 10^{-4}$ and 10^{-3}) have significantly reduced vertical impact velocities because they are able to effectively respond to the fluid and reduce their approach speed as v_f reduces to satisfy the boundary conditions imposed by the wall. The highest vertical impact velocity (about $-0.22u_\tau$) is given by the $St^+ = 27$ particles, which is approximately consistent with the $v'_{f\text{rms}}$ near the transverse injection location. This indicates that the vertical velocity fluctuations drive these particles to the wall and that their inertia is sufficiently large that no appreciable deceleration is experienced before reaching $y^+ = 1$. As mentioned with respect to Fig. 6a, these particles have an effective Stokes number (St_Λ) of order unity, indicating that they are large enough to experience substantial velocity deviations from the largest near-wall eddies (with significant turbophoresis) but are not too large to be unresponsive to the vertical velocity fluctuations toward the wall. These results are similar to those of Uijttewaal and Oliemans,[25] except for the highest St^+ case, where, again, the present near-wall injection condition yields a reduced impact velocity in comparison.

Finally, consider the approach angle of the particles to characterize the near-wall trajectories. This angle can be related to the ratio

of vertical to horizontal bounce velocity, as shown in Fig. 8c. The results show that the particles approach the wall at a shallow angle and that this angle increases with x^* for the two large inertia cases (to about 2 deg), consistent with the results of Uijttewaal and Oliemans.[25] The smaller inertia particles (which have $St_\Lambda \ll 1$) yield an approximately constant impact angle of about 0.5 deg, which is attributed to the finite u_{bounce} of Fig. 8a stemming from the $y^+ = 1$ reflection.

D. Statistics Along the Particle Trajectory

The Lagrangian-averaged transverse particle velocities from the DNS results are compared to a model that neglects effects of turbulent diffusion in Fig. 9a. The zero-turbulence model is found by integrating the particle equation of motion in the mean velocity field such that the particle vertical velocity is the sum of only gravitational effects and the mean vertical velocity, that is, $V_{term} + \langle\overline{v_f}\rangle$. The DNS results show that at low particle inertias, the transverse velocity includes a substantial upward drift that is manyfold of the terminal velocity, indicating that turbulent diffusion mechanisms predominately drive the particles away from the wall. This effect is reduced at high inertias, for example, the largest particle case ($St_\delta = 1$) yields a $\langle v_p\rangle / V_{term}$ of about two, and one would expect that a further increase in St_δ would yield the asymptotic value of V_{term} for $\langle v_p\rangle$. From the model prediction, note that neglecting turbulent diffusion is wholly ineffective at predicting the mean transverse particle movement, except for the highest Stokes number case, and that the influence of $\overline{v_f}$ is secondary at most. The importance of diffusion in the Lagrangian mean particle velocity is reinforced when comparing these data to those of the zero-turbulence model predictions. A second model by Dorgan[18] was also explored that accounts for the influence of turbulence by adding the effect of homogeneous turbulent diffusion (based on the model of Hinze[22]) and the nonhomogeneous turbophoresis velocity (based on a model by Young and Leeming[4]). It was found that the model was only able to reproduce the DNS trends in a qualitative sense, and the differences were attributed to inhibited downward diffusion (because the wall limits the maximum downward travel and also creates upward bouncing velocities).

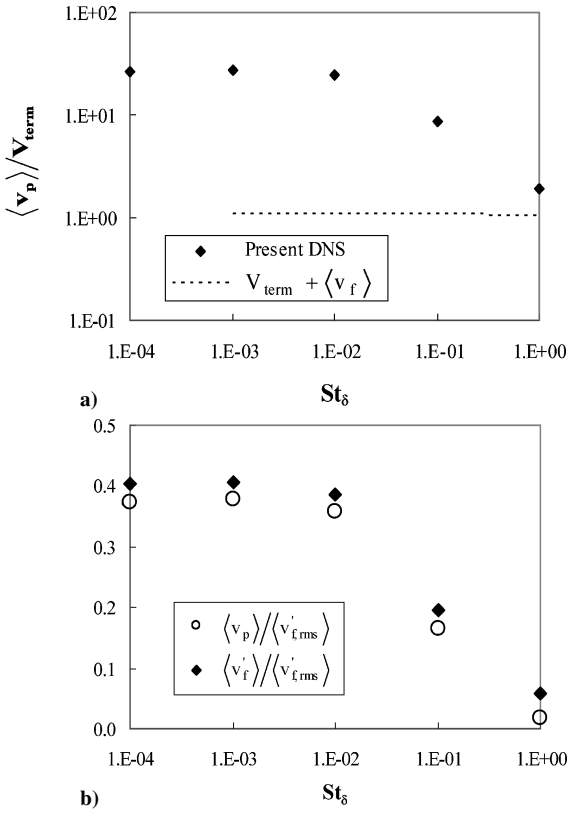

Fig. 9 Lagrangian-averaged vertical velocities: a) particle velocity for DNS and zero-turbulence simulations normalized by V_{term} and b) particle velocity and fluid velocity deviation from mean Eulerian value normalized by $\langle v'_{f,rms}\rangle$.

Because the aforementioned upward drift is attributed to fluid turbulence, it is interesting to evaluate the mean Lagrangian fluid velocity $\langle v_f\rangle$ that the particle "sees" because it is expected to deviate significantly from the small Eulerian fluid velocity $\overline{v_f}$. The fluid velocity along the particle path can be decomposed into a mean and a drift component, that is, $\langle v_f\rangle = \langle v'_f + \overline{v_f}\rangle = \langle v'_f\rangle + \langle\overline{v_f}\rangle$. The perturbation at any point in time for a particle is, thus,

$$v'_f(x_p, y_p, z_p, t_p) = v_f(x_p, y_p, z_p t_p) - \overline{v_f(x_p, y_p)} \tag{9}$$

from which the mean fluid velocity drift $\langle v'_f\rangle$ can be obtained by averaging over all trajectories and over all particles. Although an Eulerian (or moving Eulerian) average of the perturbation will be zero based on its definition, that is, $\overline{v'_f} \equiv 0$, it can be finite in a Lagrangian particle-path frame. In particular, if particles are carried away from the wall by turbulent diffusion, this must be accompanied by a mean vertical component drift, that is, $\langle v'_f\rangle > 0$. This is consistent with the results shown in Fig. 9b, which are normalized by the Eulerian transverse turbulence intensity averaged along the particle path, $\langle v'_{f,rms}\rangle = \langle v'_{f,rms}(x_p, y_p)\rangle$. The smallest particles ($St_\delta = 10^{-4}$) have drifts approaching 40% of the transverse turbulence intensity observed along their path. This is caused by the asymmetric diffusion due to the near-wall injection, whereby downward diffusion is limited, whereas upward diffusion is unlimited. (The wall boundary condition combined with the chosen injection location does not allow much downward travel.) For the highest inertia case ($St_\delta = 1$), the influence of diffusion is weaker because the particle trajectories are unresponsive to much of the turbulence (especially in the near-wall region). Therefore, these particles are likely to behave as if moving in an Eulerian reference frame, where the $\langle v'_f\rangle$ should approach zero as Stokes number increases, which is the trend that is seen. Some qualitatively similar results have been reported by Narayanan et al.[10] but differ substantially due to different injection conditions.

Figure 9b also shows the vertical particle velocity, where it noted that there is a high degree of correlation between $\langle v_p\rangle$ and $\langle v'_f\rangle$ for all cases. Thus, the mean transverse movement of the particle cloud is primarily controlled by turbulent diffusion for the low and intermediate Stokes number cases, and this explains the large values of $\langle v_p\rangle / V_{term}$ shown in Fig. 9a. Note that relative velocity effects become more important as the particle inertias become large ($St^+ \gg 1$), but do not seem to be simply quantified by a terminal velocity. The relative velocity statistics are explored more in the next section.

E. Relative Particle Velocity Statistics

In the following text, the fluctuations of the particle relative velocity from the Lagrangian average is considered. These can be defined for the transverse velocity as

$$\langle v_{rel,rms}\rangle = \left\{\left\langle v_{rel}^2\right\rangle - \langle v_{rel}\rangle^2\right\}^{\frac{1}{2}} \tag{10}$$

Figure 10a shows rms of various components of the relative velocity fluctuations about the Lagrangian mean, which are normalized by their respective Eulerian fluid turbulence levels. If the particles' relative velocity were not significantly affected by the turbulence, that is, if the particles approximately moved at V_{term} with respect to the fluid at all times (which is the asymptote as Stokes number approaches zero), then the rms components of the relative velocity would approach zero. For both relative velocity components, the Lagrangian rms values diminish as Stokes number decreases, which is consistent with this limit.

However, as the particles' inertia increases, the rms values of the relative velocity fluctuations are much larger than V_{term}, and the values eventually becomes on the order of the local turbulence intensity. This is because the larger particles (which can be called inertia-dominated particles because $St^+ \gg 1$ and $\gamma \ll 1$) tend to act as moving-Eulerian elements, which will experience relative velocity fluctuations on the order of the fluctuations in the fluid velocity.[15]

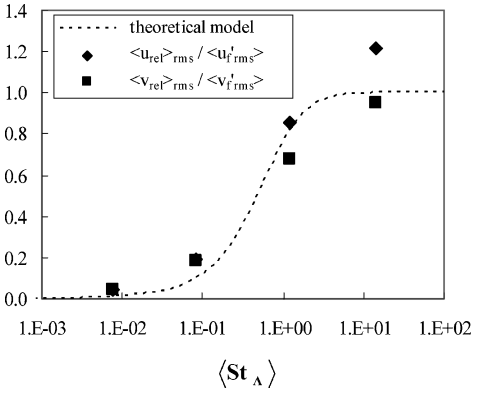

Fig. 10a Relative fluid velocity fluctuations.

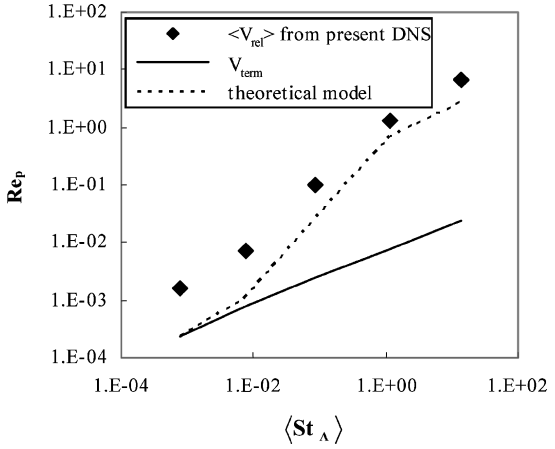

Fig. 10b Reynolds number obtained from DNS statistics compared with a theoretical model.

This phenomenon can be described by considering a particle subjected to a simple sinusoidal fluctuation, for example, given by $v_f(t) = \alpha \sin(2\pi t/\tau_f)$, where α is the amplitude of the fluid velocity fluctuations and τ_f is the time period of the oscillations. By integration of the particle equation of motion (3), and under the assumption of independence of the initial conditions, the time evolution of the particle's relative velocity is given by

$$V_{\text{rel}}(t) = -\frac{2\pi(\text{St})\alpha}{1+4\pi^2(\text{St})^2}\cos\left(\frac{2\pi t}{\tau_f}\right) + \left(\frac{\alpha}{1+4\pi^2(\text{St})^2} - \alpha\right)\sin\left(\frac{2\pi t}{\tau_f}\right) + V_{\text{term}} \tag{11}$$

where $\text{St} = \tau_p/\tau_f$, which is a Stokes number for the sinusoidal fluctuation. Averaging over a time corresponding to an integer of the sinusoidal period gives the mean V_{term} for this simple flow. However, the rms of the relative velocity fluctuations about the mean is

$$\frac{v_{\text{rel,rms}}}{v'_{f,\text{term}}} = \left(\left\{\frac{\text{St}_\Lambda \cos^{-1}(1/e)}{1+\text{St}_\Lambda^2[\cos^{-1}(1/e)]^2}\right\}^2 + \left\{\frac{1}{1+\text{St}_\Lambda^2[\cos^{-1}(1/e)]^2} - 1\right\}^2\right)^{\frac{1}{2}} \tag{12}$$

where $\text{St}_\Lambda = 2\pi\,\text{St}/[\cos^{-1}(1/e)]$ by assuming an exponential decay for the decorrelation timescale and where $\alpha/\sqrt{2} = v'_{f\text{rms}}$ has been used to characterize the strength of the fluctuations. Similarly, we can examine the velocities perpendicular to the terminal velocity and find that the mean will be zero, but the ratio of the rms velocities will be the same function of the integral Stokes number as in Eq. (12), that is, $(u_{\text{rel,rms}}/u'_{f\text{rms}}) = (v_{\text{rel,rms}}/v'_{f\text{rms}})$. This simple theory is shown in Fig. 10a with comparison to the Lagrangian DNS data of both transverse and streamwise fluctuations, and the agreement is quite reasonable. For the limit of $\text{St}_\Lambda \gg 1$ and $v'_{f,\text{rms}}$ and $u'_{f,\text{rms}} \gg V_{\text{term}}$, which corresponds to inertia-dominated particles, the simple model gives $v_{\text{rel,rms}} = v'_{f,\text{rms}}$ and $u_{\text{rel,rms}} = u'_{f,\text{rms}}$, which is consistent with the trend for the DNS data. As such, particles with large response times and small drift parameters can be expected to experience relative velocity fluctuations that are on the order of the fluctuations in the turbulence (and much larger than the particle's terminal velocity). This is significant in that the magnitude of the instantaneous relative velocity at these high inertias (and small γ) will be dominated by the surrounding fluid turbulence and not the gravitational forces.

Figure 10b gives the average particle Reynolds number based on the Lagrangian-averaged relative velocity magnitude $\langle|V_{\text{rel}}|\rangle$ and the terminal particle Reynolds number based on V_{term}. These two Reynolds numbers are defined as

$$\langle Re_p\rangle = \langle|V_{\text{rel}}|\rangle d/v_f, \qquad Re_{p\text{term}} = V_{\text{term}} d/v_f \tag{13}$$

The typical Re_p values are generally less than unity and demonstrate that the use of a linear drag law for these particles is reasonable. In general, an increase in Stokes number is associated with a linear increase in $Re_{p,\text{term}}$ on the log–log scale, with a slope of one-half, because the fluid viscosity was held constant and the particle diameter varies with $\sqrt{\tau_p}$. However, as the Stokes number increases, the path-averaged Re_p based on the DNS results are much larger than those based on V_{term}. To explain this, the theoretical model curve shown in Fig. 10b was computed by assuming that

$$V_{\text{rel}}^2 = V_{\text{term}}^2 + V_{\text{rel,rms}}'^2 \tag{14}$$

where $V_{\text{rel,rms}}^2 = u_{\text{rel,rms}}^2 + v_{\text{rel,rms}}^2$ and where the rms components were based on Eq. (12). As seen in Fig. 10b, the theoretical model reasonably represents the DNS data and indicates that inertia-dominated particles can be subjected to mean Re_p values that far exceed $Re_{p,\text{term}}$.

In summary, strong relative velocities fluctuations were found in the Lagrangian mean that approached the local turbulent fluctuations in the fluid (and far exceeded V_{term}) for inertia-dominated particles ($\text{St}^+ \gg 1$ and $\gamma \ll 1$). These trends were predicted by a simple model, indicating that $Re_{p,\text{term}}$ alone is a poor guide for determining the particle Re_p for the present test conditions and that turbulent fluctuations effects should be included for high Stokes numbers.

IV. Conclusions

Simulations have been conducted for a range of particle inertias for a fixed and finite terminal velocity in a DNS resolved turbulent boundary layer. Preferential concentration was noted for all inertia values near the initial release point; however, far downstream, the phenomenon was strongest for $\text{St}^+ \approx 3$ whereas it weakened for lower Stokes numbers or was restricted to long streaks for larger Stokes numbers. The reflection condition also yielded more diffuse streaks than seen in previous DNS channel flow studies. Little difference was seen in the particle concentration profiles for $\text{St}^+ < 1$, indicating that these particles behave as fluid scalars. Particles with larger inertia yielded a decreased diffusion from the wall because the particles were more likely to be trapped by boundary-layer sweeps than removed by boundary-layer ejections.

Because of the near-wall injection, particle–wall collisions were seen to increase with downstream position and St^+ until the particle cloud becomes sufficiently diffused, at which point the frequency tended to become approximately constant, whereupon the resulting collision rates were similar to channel flow deposition for uniform injection. The particle impacts were characterized by low approach angles (2 deg or less) and streamwise impact velocities on the order of the friction velocity. This was qualitatively similar to previous channel-flow deposition studies, but differences due to near-wall injection were noted for the largest particles and differences due to wall reflections were noted for the smallest particles.

The mean transverse movement of the particle cloud transitioned from that controlled by fluid-tracer asymmetric diffusion for the

smallest particles ($St^+ < 1$) to a gravitationally controlled vertical movement for the largest particles ($St^+ \gg 1$). However, the relative velocity was not well represented by a simple steady terminal velocity. In particular, the fluctuations of the mean Lagrangian relative velocity were also found to be small for the lowest-inertia particles but approached the local turbulent fluctuations in the fluid (and far exceeded V_{term}) for inertia-dominated particles ($St^+ \gg 1$ and $\gamma \ll 1$), as demonstrated by a simple model. Consequently, these inertia-dominated particles were subjected to mean Re_p that far exceeded $Re_{p,\text{term}}$.

Acknowledgments

This material is based on work supported by the Defense Advanced Research Projects Agency under Grant MDA972-01-C-0042, with Lisa Porter as Project Manager. Additionally, facilities provided by the National Partnership for Advance Computational Infrastructure were utilized for the direct numerical simulations.

References

[1]Stock, D. E., "Particle Dispersion in Flowing Gases—1996 Freeman Scholar Lecture," *Journal of Fluids Engineering*, Vol. 118, No. 7, 1996, pp. 4–17.

[2]Groszmann, D. E., Fallon, T. E., and Roger, C. B., "Decoupling the Roles of Inertia and Gravity on the Preferential Concentration of Particles," American Society of Mechanical Engineers, Paper FEDSM99-7871, New York, 1999.

[3]Loth, E., "Numerical Approaches to Dilute Two-Phase Flow," *Progress in Energy and Combustion Science*, Vol. 26, No. 3, 2000, pp. 161–223.

[4]Young, J., and Leeming, A., "A Theory of Particle Deposition in a Turbulent Pipe Flow," *Journal of Fluid Mechanics*, Vol. 340, 1997, pp. 129–159.

[5]Friedlander, S. K., and Johnstone, H. F., "Deposition of Suspended Particles from Turbulent Gas Streams," *Industrial and Engineering Chemistry*, Vol. 49, No. 7, 1957, pp. 1151–1156.

[6]McLaughlin, J. B., "Aerosol Particle Deposition in Numerically Simulated Channel Flow," *Physics of Fluids*, Vol. 1, No. 7, 1989, pp. 1211–1224.

[7]Brooke, J. W., Kontomaris, K., Hanratty, T. J., and McLaughlin, J. B., "Turbulent Deposition and Trapping of Aerosols at a Wall," *Physics of Fluids A*, Vol. 4, No. 4, 1992, pp. 825–834.

[8]Pedinotti, S., Mariotti, G., and Banerjee, S., "Direct Numerical Simulation of Particle Behavior in the Wall Region of Turbulent Flows in Horizontal Channels," *International Journal of Multiphase Flow*, Vol. 18, No. 6, 1992, pp. 927–941.

[9]van Haarlem, B., Boersma, B. J., and Nieuwstadt, F. T. M., "Direct Numerical Simulation of Particle Deposition onto a Free-Slip and No-Slip Surface," *Physics of Fluids*, Vol. 10, No. 10, 1998, pp. 2608–2620.

[10]Narayanan, C., Lakehal, D., Botto, L., and Soldati, A., "Mechanisms of Particle Deposition in a Fully Developed Turbulent Open Channel Flow," *Physics of Fluids*, Vol. 15, No. 3, 2003, pp. 763–775.

[11]Marchioli, C., and Soldati, A., "Mechanisms for Particle Transfer and Segregation in a Turbulent Boundary Layer," *Journal of Fluid Mechanics*, Vol. 468, 2002, pp. 283–315.

[12]Kallio, G. A., and Reeks, M. W., "A Numerical Simulation of Particle Deposition in Turbulent Boundary Layers," *International Journal of Multiphase Flow*, Vol. 15, No. 3, 1989, pp. 433–446.

[13]Liu, B. Y. H., and Agarwal, J. K., "Experimental Observation of Aerosol Deposition in Turbulent Flow," *Aerosol Science*, Vol. 5, 1974, pp. 145–155.

[14]Crowe, C., Sommerfeld, M., and Tsuji, Y., *Multiphase Flows with Droplets and Particles*, CRC Press, Boca Raton, FL, 1998.

[15]Loth, E., and Stedl, J., "Taylor and Lagrangian Correlations in a Turbulent Free Shear Layer," *Experiments in Fluids*, Vol. 26, No. 1, 1999, pp. 1–6.

[16]Wang, L.-P., and Maxey, M. R., "Settling Velocity and Concentration Distribution of Heavy Particles in Homogeneous Isotropic Turbulence," *Journal of Fluid Mechanics*, Vol. 256, 1993, pp. 27–68.

[17]Aliseda, A., Cartellier, A., Hainaux, F., and Lasheras, J. C., "Effect of Preferential Concentration on the Settling Velocity of Heavy Particles in Homogeneous Isotropic Turbulence," *Journal of Fluid Mechanics*, Vol. 468, 2002, pp. 77–105.

[18]Dorgan, A. J., "Particle Dispersion Near the Upper Wall of a Turbulent Boundary Layer," M.S. Thesis, Dept. of Aeronautical and Astronautical Engineering, Univ. of Illinois, Urbana, IL, Dec. 2003.

[19]Kaftori, D., Hetsroni, G., and Banerjee, S., "Particle Behavior in the Turbulent Boundary Layer. II. Velocity and Distribution Profiles," *Physics of Fluids*, Vol. 7, No. 5, 1995, pp. 1107–1121.

[20]Bocksell, T. L., "Numerical Simulation of Turbulent Particle Diffusion," Ph.D. Dissertation, Dept. of Aeronautical and Astronautical Engineering, Univ. of Illinois, Urbana, IL, Dec. 2003.

[21]Spalart, P. R., and Watmuff, J. H., "Experimental and Numerical Study of a Turbulent Boundary Layer with Pressure Gradients," *Journal of Fluid Mechanics*, Vol. 249, 1993, pp. 337–371.

[22]Hinze, J. O., *Turbulence*, McGraw–Hill, New York, 1959, Chap. 5.

[23]Barton, I. E., "Exponential-Lagrangian Tracking Schemes Applied to Stokes Law," *Journal of Fluids Engineering*, Vol. 118, 1996, pp. 85–89.

[24]Soltani, M., and Ahmadi, G., "Direct Numerical Simulation of Particle Entrainment in Turbulent Channel Flow," *Physics of Fluids A*, Vol. 7, No. 3, 1995, pp. 647–657.

[25]Uijttewaal, W. S. J., and Oliemans, R. V. A., "Particle Dispersion and Deposition in Direct Numerical and Large Eddy Simulations of Vertical Pipe Flows," *Physics of Fluids*, Vol. 8, No. 10, 1996, pp. 2590–2604.

J. Bellan
Associate Editor